Research Article Vol. 60, No. 26 / 10 September 2021 / Applied Optics 7929

applied optics

Experimental identification of a grating profile using neural network classifiers in optical scatterometry

Moustapha Godi Tchéré,[1,*] Stéphane Robert,[1] Zaki Sabit Fawzi,[2] Bernard Bayard,[1] Damien Jamon,[1] and Cécile Gourgon[3]

[1]Université de Lyon, Université Jean Monnet de Saint-Etienne, Laboratoire Hubert Curien, 42000 Saint-Etienne, France
[2]Ecole Nationale Supérieure des Technologies de l'Information et de la Communication (ENASTIC), BP:5363 N'Djamena, Chad
[3]Université Joseph Fourier de Grenoble, Laboratoire des Technologies de la Microélectronique, 38054 Grenoble, France
*Corresponding author: godi.tchere.moustapha@univ-st-etienne.fr

Received 8 June 2021; revised 3 August 2021; accepted 3 August 2021; posted 5 August 2021 (Doc. ID 432987); published 2 September 2021

In this paper, we develop a new technique, to the best of our knowledge, of grating characterization based on two separate steps. First, an artificial neural network (ANN) is implemented in a classifier mode to identify the shape of the geometrical profile from a measured optical signature. Then, a second ANN is used in a regression mode to determine the geometrical parameters corresponding to the selected geometrical model. The advantage of this approach is highlighted by discussions and studies involving the error criterion that is used widely in scatterometry. In addition, experimental tests are provided on diffraction grating structures with a period of 500 and 750 nm.

https://doi.org/10.1364/AO.432987

1. INTRODUCTION

The size reduction of electronic chips in processors and sensors has enabled the development of many applications in the fields of telecommunications, electronics, and optics. Manufacturing of these miniaturized electronic components requires fast and accurate characterization tools. Conventional techniques such as atomic force microscopy (AFM) and scanning electron microscopy (SEM) have shown their limitations in resolution, and some are even destructive. The classical technique based on the resolution of an inverse scattering problem has been highly developed to reduce these restrictions [1]. Scatterometry is a fast, accurate, and non-destructive technique. It operates in two stages: the measurement of optical signatures and treatment. The optical signature is mainly obtained by a reflectometer [2] or an ellipsometer [3]. The treatment of the optical signature can be solved by different methods, such as classical optimization [4], a metaheuristic technique [5], a library search [6], or an artificial neural network (ANN) [7]. Many works have demonstrated the effectiveness of the latter and its significant resistance to noise measurement [8].

Solving the inverse problem in scatterometry requires essential prior knowledge of the geometrical shape of the structure to be tested. The initial condition involves fixing the profile shape of the structure throughout the entire characterization process. The deviation of an actual shape from the expected one is a well-known problem giving rise to greater or less significant characterization errors. Thus, different works have examined the incidence of different defects of profile shape occurring throughout the fabrication process. In [9], the authors implement a generic profile to adjust the deviation from the nominal shape as closely as possible. However, the number of geometrical parameters is significantly increased, leading to a more complex inverse problem to solve. In [10], a new approach to characterizing a complex profile by a combination of several geometrical profiles was introduced, and this technique requires separate characterizations with all available shapes.

In addition, different works have demonstrated the ability to identify a particular defect on a manufactured sample from the treatment of the optical signature. In [8], the authors demonstrate the ability of a neural network to detect a residual layer considered to be a mask defect in lithography from an ellipsometric signature. In [11], we implement a self-organizing map (SOM) to detect a residual layer under the mask during a photolithographic process. These theoretical works require further experimental validations. In [12,13], the authors combine a support vector machine method with a library search to identify the deviation of the geometrical profile from a trapezoidal one.

In this paper, a solution is proposed to unambiguously validate the fixed shape during a complete characterization process, fully achieved using neural networks. We suggest an ANN to identify the shape of the geometrical profile from a fixed optical signature. Then, a second ANN is used to extract the geometrical parameters corresponding to the structure from the same previous measurement. This paper is organized as follows.

Section 2 introduces the context of ellipsometric scatterometry. It briefly describes the principle of ellipsometric measurement, the numerical simulation of the optical signatures, and the structure of the actual samples used in this work. The models of the different geometrical profiles used are also defined. Section 3 describes the operation mode of a classical ANN used in scatterometry. It also provides its performances in characterization. Then, a classifier based on a particular ANN is used to identify the geometrical profile of the structure in Section 4. Experimental results are supplied to investigate the effectiveness of the method in real conditions. Finally, Section 5 presents the results of a complete characterization method.

2. CONTEXT OF THE STUDY

A. Measurement of the Optical Signature

In ellipsometric scatterometry, the optical signature is based on the measurement of the conventional angles ψ and Δ for different wavelengths for a fixed structure. The determination of ellipsometric angles is detailed in [14]. In this work, a phase modulator spectroscopic ellipsometer is employed. It measures the intensities I_s and I_c depending on these ellipsometric angles by

$$Is = \sin 2\psi \sin \Delta, \tag{1}$$

$$Ic = \sin 2\psi \cos \Delta. \tag{2}$$

Thus, the optical signature is subsequently defined by the intensities I_s and I_c, measured for a fixed range of wavelengths.

To train the ANNs used in this paper, large sets of theoretical samples included in a fixed range of corresponding parameters were generated. Corresponding optical signatures (I_s and I_c) were simulated via the multilayer modal method by Fourier expansion [15] on a wavelength spectrum ranging from 278 to 1771 nm, in a step of 19.7 nm (i.e., 152 values) with an incidence angle of 70°. Gaussian noise corresponding to the disturbance of an experimental measurement ($3\sigma = 0.01$) was hence introduced. Studied gratings are composed of a fixed resist layer deposited on a bottom anti-reflective coating (BARC) (DUV30) based on a silicon dioxide (SiO_2) layer, all placed on silicon substrate (Fig. 1). The layer of BARC is added to minimize the intensity of reflected light from the silicon substrate. The BARC and SiO_2 thicknesses are 49 and 50 nm, respectively.

Gratings called E_1, E_2, E_3, and E_4, respectively, are manufactured to experimentally validate this study. Figure 2 depicts a cross-sectional SEM image of each sample.

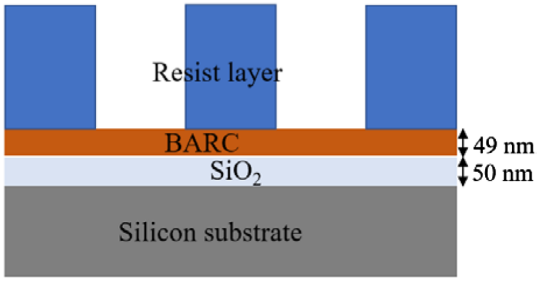

Fig. 1. Geometrical structure of grating used in the study.

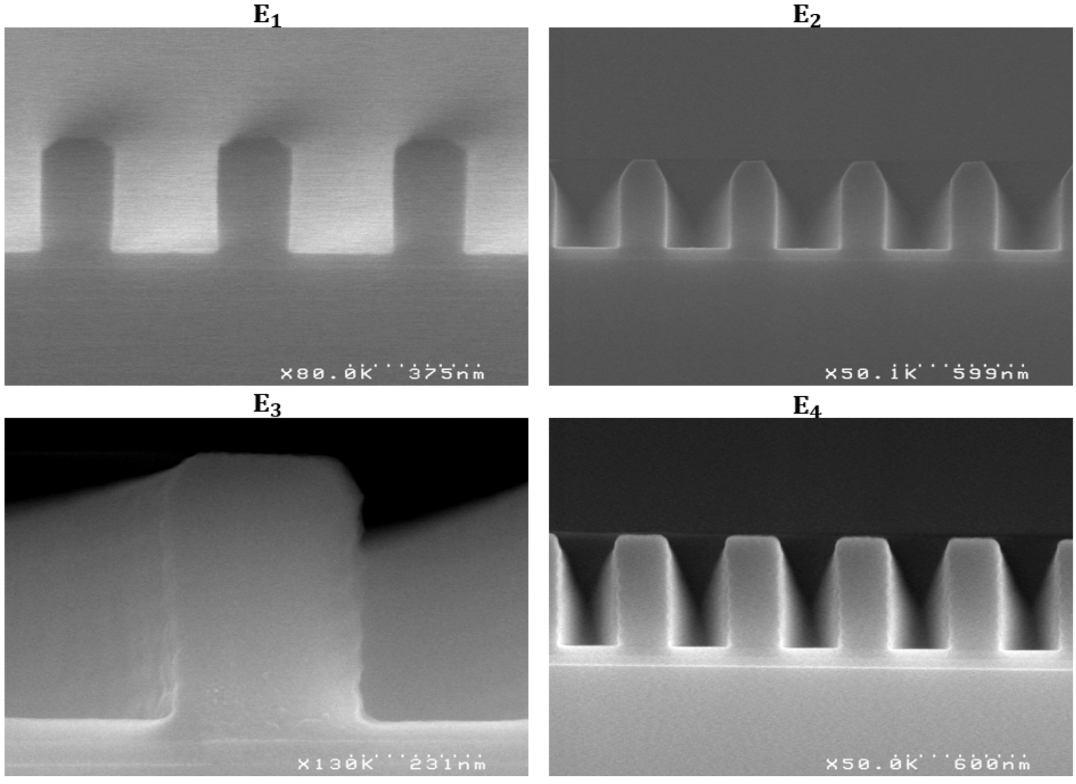

Fig. 2. Cross-sectional SEM view of resist gratings E_1, E_2, E_3, and E_4.

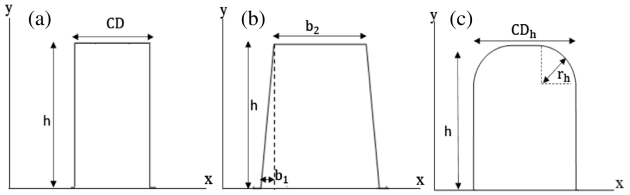

Fig. 3. Geometrical parameters of theoretical profiles widely used in scatterometry: (a) rectangular, (b) trapezoidal, and (c) rectangular rounded at the top.

B. Definition of the Geometrical Profiles

A set of profiles widely used in scatterometry is defined in the following to best adjust the actual form of the experimental samples. The rectangular shape [Fig. 3(a)] defined by two parameters is the simplest. It is usually considered as the expected profile. The other profiles represent different types of defects. The popular symmetric trapezoidal shape involving three parameters [Fig. 3(b)] is usually employed in scatterometry to include a particular deviation from the rectangular one. Finally, the rectangular shape rounded at the top implies an additional parameter r_h [Fig. 3(c)]. However, it is replaced by the following normalized coefficient δ $(0 < \delta < 1)$ to ensure a fixed variation range:

$$\delta = \frac{2 * r_h}{CD_h}. \tag{3}$$

3. CLASSICAL CHARACTERIZATION

A. ANN Applied in the Regression Mode

In scatterometry, the geometrical parameters corresponding to a fixed shape can be estimated by an ANN operating in the regression mode. Hence, it is possible to learn the relationship from a correlated dataset $\{X, Y\}$. In our case, $X = \{x_1, x_2, \ldots, x_M\}$ represents the geometrical parameters defining the profile shape of the sample, and $Y = \{y_1, y_2, \ldots, y_n\}$ gives its corresponding optical signature. The training is performed with respect to fixed conditions such as experimental configurations of measurement or assigned profile shape. Then, the ANN can predict outputs (i.e., the geometrical parameters X) from a new input Y (i.e., the optical signature), resolving the inverse scattering problem in the specified requirements.

In our work, a multilayer perceptron (MLP) (Fig. 4) is implemented. It is composed of interconnected neurons distributed into three layers. The neurons are connected from inputs to outputs. Each connection is assigned with synaptic weights. The coefficient $w_{j,i}$ links the connection between the ith element of the input vector and the jth neurons of the hidden layer, and $z_{m,j}$ defines the connection between the jth hidden neuron and the mth output neuron. The states p_j and s_m of neurons j and m are calculated using the following equations:

$$p_j = f\left(\sum_{i=0}^{n} w_{j,i} y_i\right), \tag{4}$$

$$s_m = g\left(\sum_{j=0}^{N} z_{m,j} p_j\right), \text{ with } y_0 = 1, \tag{5}$$

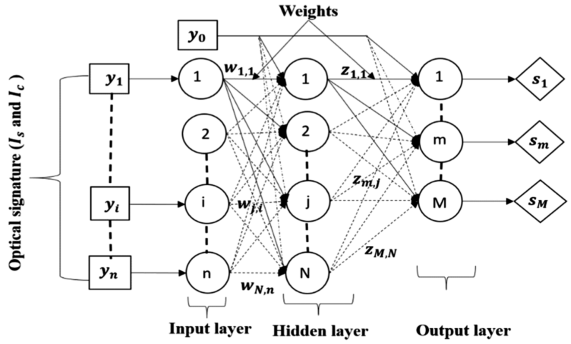

Fig. 4. Architecture of a multilayer perceptron. Inputs are the optical signatures of the sample, and outputs correspond to estimated geometrical parameters of the structure.

where f and g are the activation functions of the neurons in the hidden layer and the output one, respectively, defined as

$$f(x) = \frac{1}{1 + e^{-x}}, \tag{6}$$

$$g(x) = x. \tag{7}$$

The implemented ANN regression operates with supervised training. This process consists og adjusting the weights $w_{j,i}$ and $z_{m,j}$ to minimize the squared error e between the targets values X and the estimated ones $S = \{s_1, s_2, \ldots, s_M\}$ for a particular set of samples of the training corpus.

The final performance is evaluated using the root mean square error calculated on each output s_m (E^m_{rmse}) on a particular simulated dataset (n_{test}), not included in the training corpus:

$$E^m_{\text{rmse}} = \sqrt{\frac{1}{n_{\text{test}}} \sum_{k=1}^{n_{\text{test}}} (s^k_m - x^k_m)^2}, \tag{8}$$

where k represents the number of samples.

Differently implemented MLP are nominated as follows: MLP_R_1 for the determination of a rectangular profile, MLP_R_2 for the trapezoidal one, and MLP_R_3 for the rectangular one rounded at the top. Each MLP contains an optimal number of hidden neurons supplied by preliminary results. For example, the MLP_R_3 contains 15 neurons in the hidden layer. Each corresponding geometrical parameter ranges in the domains indicated in Table 1. In addition, each MLP is trained on 3000 datasets with the following repartition: 70% (2100) for training, 15% (450) for validation, and 15% (450) for test.

The performances of the MLPs [Eq. (8)] were systematically calculated from 450 random samples included in the training set but not used for the learning phase. Results are outlined in Table 2.

Table 1. Geometrical Parameter Ranges for the MLP_R_1, MLP_R_2, and MLP_R_3 Training

MLP_R_1	MLP_R_2	MLP_R_3
150 nm < CD < 250 nm	5 nm < b_1 < 30 nm130 nm < b_2 < 220 nm	0.1 < δ < 1120 nm < CD_h < 250 nm
250 nm < h < 420 nm	250 nm < h < 420 nm	250 nm < h < 420 nm

Table 2. Performances of the Differently Trained MLPs: MLP_R$_1$, MLP_R$_2$, and MLP_R$_3$

MLP_R$_1$	MLP_R$_2$	MLP_R$_3$
$E_{rms}^{CD} = 0.03$ nm	$E_{rms}^{b1} = 0.18$ nm	$E_{rms}^{\delta} = 0.01$
$E_{rms}^{h} = 0.03$ nm	$E_{rms}^{b2} = 0.30$ nm	$E_{rms}^{CD_h} = 0.66$ nm
	$E_{rms}^{h} = 0.22$ nm	$E_{rms}^{h} = 0.40$ nm

B. Experimental Results of the ANN Applied in Regression

In this section, the experimental sample E_1 depicted in Section 2.A is characterized by the ANN detailed previously. The measured optical signature of the sample E_1 (Fig. 2) is provided to different MLPs to achieve characterization. Table 3 presents the corresponding results.

The quality of the characterization is popularly evaluated using the mean square error (E_{I_s,I_c}) [6,9,10,16] on optical signatures calculated between the measured intensities (I_{measured}) and the simulated ones from the S results of the ANN ($I_{\text{simulated}}$):

$$E_{Is,Ic} = \sqrt{\frac{1}{N_m}\sum_{i=1}^{N_m}(I_{\text{measured}} - I_{\text{simulated}})^2}, \tag{9}$$

where N_m represents the number of measures potentially different from n.

First, different ANNs provide geometrical parameters included in the training ranges except for MLP_R$_2$ and MLP_R$_3$ (b_1 and δ are relatively close to the limit of the range). Second, the errors E_{I_s,I_c} of the different ANNs are small but nearly identical. Unlike microscopic methods, the results provide no reliable information on shape discrimination. The value of the errors E_{I_s,I_c} is clearly insufficient to validate results.

We also note that the optical signatures calculated from different ANNs estimations are confused and are close to the measured optical signature (Fig. 5). Hence, in this configuration, the bijectivity is not ensured.

We propose a solution involving the implementation of an ANN in the classifier mode to provide additional information to remove this ambiguity. Thus, another ANN is considered to identify the geometrical profile, thus allowing the prior one to determine the corresponding geometrical parameters.

4. GEOMETRICAL PROFILE IDENTIFICATION

A. ANN in the Classifier Mode

An ANN can be implemented as a classifier. In this case, each geometrical shape corresponds to a class. The optical signature of the sample to be tested is provided as input. The ANN identifies one of the M classes by a binary vector $C = \{c_1, c_2, \ldots, c_M\}$ instead of S. Hence, the value of c_i represents the probability for the sample structure to belong to the ith class. The training corpus is composed of the pair $\{Y, C\}$, where Y represents the optical signature detailed in Section 2.A, and C represents the binary vector corresponding to the class of a fixed geometrical profile. The architecture of the ANN operating as a classifier is the same as that previously mentioned in Section 3.A, except for the activation function of output neurons:

$$g(x) = f(x) = \frac{1}{1+e^{-x}}. \tag{10}$$

B. On/Off Classification

In this section, an ANN classifier named MLP_C is presented. It operates in two classes. It allows a particular geometrical

Table 3. Results of the Real Sample ANN Characterization

MLP	MLP_R$_1$	MLP_R$_2$	MLP_R$_3$	SEM
Geometrical parameters	CD $= 214.04 \pm 0.03$ nm	$b_1 = 3.91 \pm 0.18$ nm	$\delta = 0.09$	$CD_{SEM} = 211$ nm
	h $= 295.49 \pm 0.03$ nm	$b_2 = 205.59 \pm 0.30$ nm	$CD_h = 212.1 \pm 0.66$ nm	$h_{SEM} = 313$ nm
		h $= 299.6 \pm 0.22$ nm	h $= 298.93 \pm 0.40$ nm	
Quality of characterization	$E_{Is,Ic} = 0.059$	$E_{Is,Ic} = 0.059$	$E_{Is,Ic} = 0.056$	

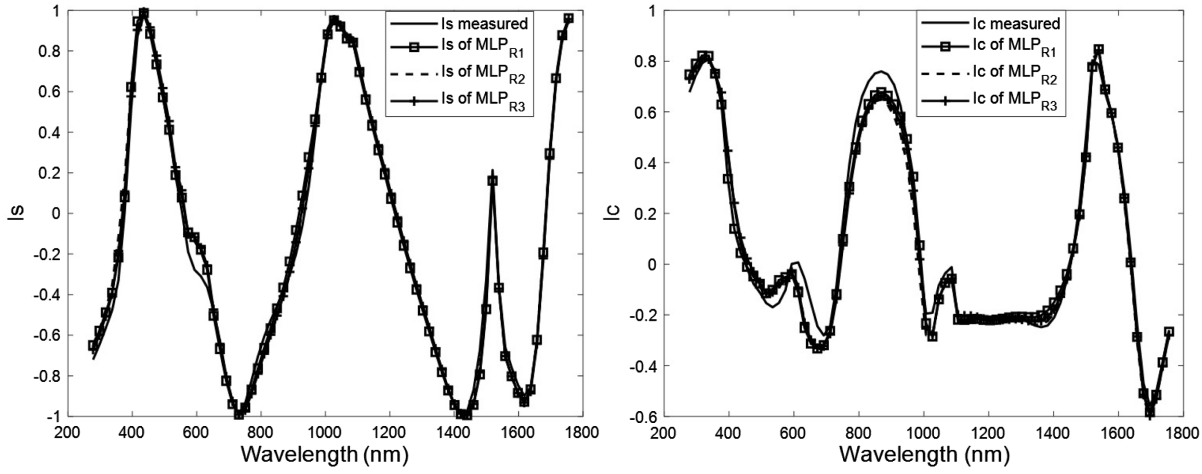

Fig. 5. Representation of the measured optical signature (Is and Ic) of sample E_1 and of simulated samples from estimated parameters using different ANNs.

Table 4. Confusion Matrix of the MLP_C Focused to Detect the Particular Rectangular Profile Noted as C_1

		Real Class		
		C_1	C_2	Precision
Predicted class	C_1	450	28	94.1
	C_2	0	422	100%
Sensitivity		100%	93.8%	Accuracy: 96.9%

profile to be detected from the measured optical signatures. For example, class C_1 is identified as the targeted rectangular profiles. Class C_2 will then contain all other shapes (in our cases, trapezoidal and rectangular ones rounded at the top). As previously mentioned, it is important tto notice the ANN classifier estimates a probability as output. Then the experimenter can fix a threshold to assign the class of the sample. In this study, it is automatically fixed at 50%, but it can be adjusted to optimize performances.

Hence, for any given sample, the following four results are possible:

- True positive (TP): the sample belongs to class C_1, and the estimation of the classifier is correct.
- False negative (FN): the sample belongs to class C_1, and the classifier identifies the class C_2.
- False positive (FP): the sample belongs to class C_2, and the estimation of the classifier is wrongly assigning the sample to class C_1.
- True negative (TN): the sample is class C_2,, and the classifier does not make mistakes.

These results are usually collected to a confusion matrix. The more diagonal the matrix is, the better the classifier performs. The following three criteria are used to measure the performance:

- The ability of the classifier to correctly identify class C_1 is

$$\text{Precision} = \frac{\text{TP}}{\text{TP} + \text{FP}}. \tag{11}$$

- The ability to perform a correct classification for all samples in class C_1 is

$$\text{Sensitivity} = \frac{\text{TP}}{\text{TP} + \text{FN}}. \tag{12}$$

- The overall rate of correct classifications is

$$\text{Accuracy} = \frac{\text{TN} + \text{TP}}{\text{TP} + \text{TN} + \text{FP} + \text{FN}}. \tag{13}$$

To identify geometrical profiles corresponding to samples E_1 and E_2, an ANN is implemented. It is composed of 20 hidden layer neurons. The variation domains defined in Table 1 are used. Classifier MLP_C is trained globally on 6000 samples (3000 for each class C_1 and C_2). The performance of this classifier is estimated on 900 random samples included in the training set, but not used for the learning phase. Results are given in Table 4.

MLP_C shows an accuracy of 96.9%. Specifically, the precision for C_2 class is 100%, while the sensitivity for the C_1 class is 100% Thus, only 28 non-rectangular profiles are misclassified as C_1, representing 3% of the entire test corpus. Moreover, all these particular profiles are rectangular rounded at the top. This finding highlights a significant sensitivity of class C_1 to profiles with low rounding at the top. The corresponding outputs of the MPL_C are represented in Table 5. The geometrical deviation E_{geo} between each misclassified profile $h(x)$ and the associated rectangular deviation $l(x)$ are calculated by

$$E_{\text{geo}} = \int_0^T |h(x) - l(x)| \mathrm{d}x. \tag{14}$$

The largest geometrical deviation calculated is 361.42 nm^2 (optical signature S_{24} in Table 5). This value represents only 0.42% of the entire grating area. Hence, all cases considered in Table 5 are very close to a rectangular profile. Figure 6 shows the value of each raw output s_1 according to the associated geometrical deviation E_{geo}.

A significant correlation between the output s_1 and the geometrical deviation can be noted.

1. Experimental Result of MLP_C

The measured optical signatures of samples E_1 and E_2 (Fig. 2) are then introduced to the previously trained MLP_C. Table 6 shows the output results. Both samples are clearly identified as class C_2.

Table 5. Details of the ANN Row Outputs (s_1 for C_1 Class and s_2 for C_2 Class) Concerning the Set of Misclassified Profiles Supplemented by the Calculated Geometrical Deviation E_{geo}

Misclassified Signatures	**S_1**	**S_2**	**S_3**	**S_4**	**S_5**	**S_6**	**S_7**	**S_8**	**S_9**	**S_{10}**
s_1	0.92	0.86	0.86	0.83	0.72	0.95	0.96	0.76	0.57	0.8
s_2	0.08	0.14	0.14	0.17	0.28	0.05	0.04	0.24	0.43	0.2
Geometrical deviation (nm^2)	56.14	192.01	104.86	63.35	49.97	66.41	116.81	62.66	247.51	61.7
Misclassified signatures	**S_{11}**	**S_{12}**	**S_{13}**	**S_{14}**	**S_{15}**	**S_{16}**	**S_{17}**	**S_{18}**	**S_{19}**	**S_{20}**
s_1	0.59	0.75	0.88	0.9	0.52	0.81	0.75	0.69	0.83	0.83
s_2	0.41	0.25	0.12	0.1	0.48	0.19	0.25	031	0.17	0.17
Geometrical deviation (nm^2)	240.34	37.31	66.61	49.61	238.03	97.09	94.14	134.25	141.67	164.67
Misclassified signatures	**S_{21}**	**S_{22}**	**S_{23}**	**S_{24}**	**S_{25}**	**S_{26}**	**S_{27}**	**S_{28}**		
s_1	0.92	0.72	0.72	0.63	0.93	0.93	0.62	0.62		
s_2	0.08	0.28	0.28	0.37	0.07	0.07	0.38	0.38		
Geometrical deviation (nm^2)	74.38	123.11	123.66	361.42	100.15	92.12	267.75	63		

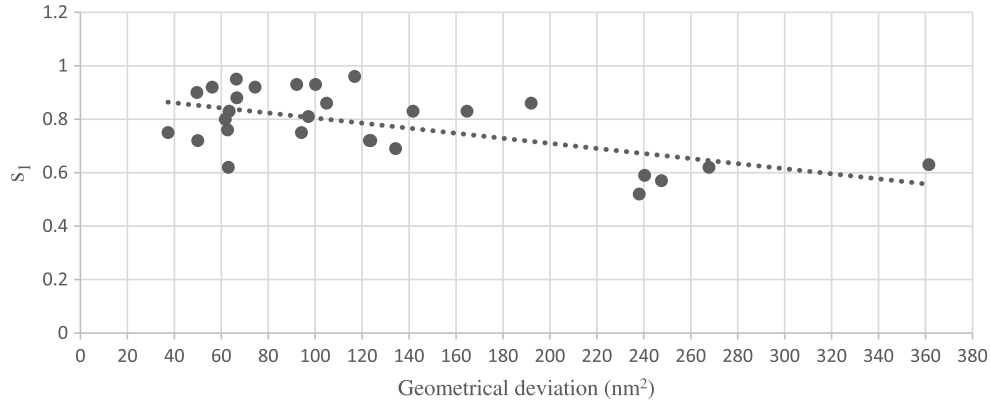

Fig. 6. Representation of the variation of raw output s_1 of MLP_C for misclassified samples according to the associated geometrical deviation.

Table 6. Output Results of the MLP_C Corresponding to Samples E_1 and E_2[a]

Optical Signatures	s_1	s_2
Sample E_1	0.00	1.00
Sample E_2	0.00	1.00

[a]Class C_1 corresponds to the rectangular profiles, and class C_2 includes all the others.

Table 7. Geometrical Parameter Ranges for Different Profile Shapes Belonging to Classes C_1, C_2, and C_3

C_1	C_2	C_3
320 nm < CD < 380 nm	10 nm < b_1 < 60 nm	0.1 < δ < 1
500 nm < h < 580 nm	260 nm < b_2 < 320 nm	320 nm < CD_h < 380 nm
	500 nm < h < 580 nm	500 nm < h < 580 nm

C. Identification of the Profile Type

In this part, an ANN classifier named MLP_P operating on three classes is presented. It can identify a particular geometrical profile among a limited number of possibilities. In our tests, class C_1 remains the rectangular profile, while classes C_2 and C_3 correspond, respectively, to the trapezoidal profile and the rectangular one rounded at the top. Each geometrical parameter ranges in the domains indicated in Table 7.

Classifier MLP_P is trained globally with 9000 samples (3000 rectangular, 3000 trapezoidal, and 3000 rectangular rounded at top). Reparation is 70% for training, 15% for validation, and 15 % for test.

The MLP_P performance is calculated from a set of 1350 random samples included in the dataset but not used for the training phase. The ANN is composed of 25 hidden layer neurons. The result is given in Table 8.

Classifier MLP_P provides excellent global performance with an accuracy of 98.6%. It guarantees maximum precision for classes C_2 and C_3 and maximum sensitivity for classes C_1 and C_2. All rectangular and trapezoidal profiles are correctly classified. Only 19 rectangular profiles rounded at the top are misclassified in C_1. This confirms the previous conclusion regarding the sensibility of this profile compared to the rectangular one (Section 4.B).

Table 8. Confusion Matrix of the MLP_P Focused to Identify a Particular Geometrical Profile[a]

		Real Class			
		C_1	C_2	C_3	Precision
Predicted class	C_1	450	0	19	95.9%
	C_2	0	450	0	100%
	C_3	0	0	431	100%
Sensitivity		100%	100%	95.8%	Accuracy: 98.6%

[a]Class C_1 corresponds to the rectangular profiles, and Classes C_2 and C_3 correspond, respectively, to the trapezoidal profile and the rectangular profile rounded at the top.

Table 9. Raw Output Results of the MLP_P for Samples E_1, E_2, E_3, and E_4

Optical Signatures	s_1	s_2	s_3
Sample E_1	0.00	0.00	1.00
Sample E_2	0.00	0.00	1.00
Sample E_3	0.00	0.00	1.00
Sample E_4	0.56	0.00	0.44

1. Experimental Results of MLP_P

The optical signatures measured for samples E_1, E_2, E_3, and E_4 (Fig. 2) are provided as inputs of classifier MLP_P to ensure experimental validation. The output results are summarized in Table 9.

The MLP_P unambiguously identifies samples E_1, E_2, and E_3 as class C_3. This third output of the MLP_P benefits from a precision of 100%. Let us consider the results concerning sample E_1 in Section 3.B. The profile shape is clearly defined by the MLP_P. Hence, the $MLP_{\_R3}$ should be selected (Table 3). In this case, this is validated by the weak value of E_{rmse}.

In contrast, the result of sample E_4 classification is more ambivalent. Indeed, the classifier indicates a slight preference for the rectangular profile to the disadvantage of the rounded one at the top. This conforms totally to the SEM image of sample E_4, which shows a rectangular shape slightly distorted at the top.

Table 10. Results of ANN Characterization of Samples E_2, E_3, and E_4 Operating in the Regression Mode for a Profile Shape Fixed by Previous Classifiers C_1 and C_3

	MLP_R_1		MLP_R_3		
Samples	Geometrical Parameters	Quality of Characterization	Geometrical Parameters	Quality of Characterization	SEM Parameters
E_2			$\delta = 0.97 \pm 0.01$ $CD = 209.61 \pm 0.66$ nm $h = 383.05 \pm 0.40$ nm	$E_{Is,Ic} = 0.12$ $E_{geoSEM\_MLPR3} = 5230.4$ nm^2	$\delta_{SEM} = 0.63$ $CD_{SEM} = 217$ nm $h_{SEM} = 383$ nm
E_3			$\delta = 0.32 \pm 0.01$ $CD = 365.88 \pm 0.66$ nm $h = 537.41 \pm 0.40$ nm	$E_{Is,Ic} = 0.16$ $E_{geoSEM\_MLPR3} = 1.474e^4$ nm^2	$\delta_{SEM} = 0.24$ $CD_{SEM} = 344$ nm $h_{SEM} = 527$ nm
E_4	$CD = 246.44 \pm 0.03$ nm $h = 559.48 \pm 0.03$ nm	$E_{Is,Ic} = 0.16$ $E_{geoSEM\_MLPR1} = 597.23$ nm^2	$\delta = 0.09 \pm 0.01$ $CD = 245.76 \pm 0.66$ nm $h = 556.76 \pm 0.40$ nm	$E_{Is,Ic} = 0.16$ $E_{geoSEM\_MLPR3} = 1251.4$ nm^2	$CD_{SEM} = 237$ nm $h_{SEM} = 562$ nm

5. COMPLETE CHARACTERIZATION

The profile shape estimated by the classifier can then be used to carry out the characterization reducing the impact of a fixed erroneous profile shape. For example, samples E_2 and E_3 have been clearly identified by the MLP_P as a rectangular profile rounded at the top. Thus, an ANN operating with a fixed shape (similar to MLP_R_1 in Section 3) is trained. Sample E_4 seems to be at the boundary between the rectangular profile and the rectangular one that is rounded at the top. The MLP_R_1 and MLP_R_3 are employed. The measured optical signature of samples E_2, E_3, and E_4 are provided to the inputs of these ANNs for characterization. The results are given in Table 10.

The MLP_R_3 estimates geometrical parameters ranked into the training range. The error E_{I_s,I_c} calculated between the measured and simulated optical signature is added to provide additional information. The estimated radius at the top is significantly large. This is consistent with the SEM image of samples E_2 and E_3 (Fig. 2).

Regarding sample E_4, the geometrical parameters estimated by MLP_R_1 and MLP_R_3 are of the same order of size. The one rounded at the top estimated by MLP_R_3 is very low and seems close to a rectangular profile. Indeed, the geometrical deviation E_{geo} calculated between the profile estimated by MLP_R_3 and the best fit, i.e., the rectangular profile with no roundness, is 52.49 nm^2. This represents only 0.03% of the entire grating area. This result is very low compared to the deviation result in Table 5. Finally, the profiles estimated by MLP_R_1 and MLP_R_3 are depicted in Fig. 7. The profiles estimated are very close. This emphasizes the results of the MLP_P (Table 9) regarding sample E_4.

In addition, geometrical parameters were roughly extracted from SEM measurements and compared to those estimated by MLP_R_1 and MLP_R_3, as reported in Table 10. We notice the geometrical deviation calculated between the MLP_R_3 profile, and the SEM of sample E_4 is 1251.4 nm^2. This seems higher, but it represents only 0.91% of the entire grating area. We think this deviation is because of the SEM scale and resolution influence on extracted parameters.

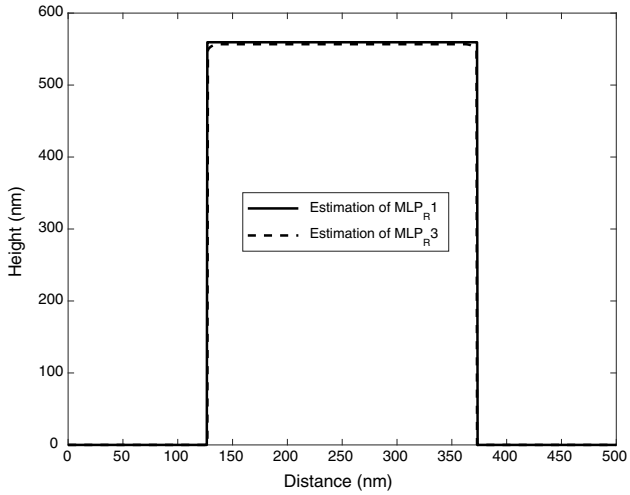

Fig. 7. Representations of the geometrical profiles obtained using different E_4 sample characterizations: MLP_R_1 (fine lines) and MLP_R_3 (dashed lines).

6. CONCLUSION

In this study, we demonstrated the common mean square errors E_{I_s,I_c} on the optical signature calculated for the reconstructed profile are clearly not sufficient to validate the quality of the characterization. Thus, a method based on a classifier is proposed to supply additional information. An ANN is aimed to collect qualitative information about the profile shape of the structure to be tested from a measured optical signature. This information is then used to reduce ambiguity on the fixed geometrical hypothesis during the characterization process. In our work, the extraction of the geometrical parameters is achieved by an ANN, but the method can be used for other techniques used in scatterometry. The method validation is demonstrated on samples with specific defects occurring throughout the manufacturing process. Moreover, the classifier can also be used efficiently alone to identify a perfect shape or a targeted structure during different stages of the manufacturing process.

Acknowledgment. The authors are grateful to P. Donnelly for stimulating discussions that have led to a more comprehensive presentation of this work.

Disclosures. The authors declare no conflicts of interest.

Data Availability. Data underlying the results presented in this paper are not publicly available at this time but may be obtained from the authors upon reasonable request.

REFERENCES

1. K. P. Bishop, S. M. Gaspar, L.-M. Milner, S. S. H. Naqvi, and J. R. McNeil, "Grating line shape characterization using scatterometry," Proc. SPIE **1545**, 64–73 (1991).
2. I. J. P. Kallioniemi and J. Saarinen, "Optical scatterometry with neural network model for nondestructive measurement of submicron features," Proc. SPIE **3743**, 33–41 (1999).
3. J. Hazart, G. Grand, P. Thony, D. Herisson, S. Garcia, and O. Lartigue, "Spectroscopic ellipsometric scatterometry: sources of errors in critical dimension control," Proc. SPIE **5041**, 9–21 (2003).
4. C. J. Raymond, M. E. Littau, A. Chuprin, and S. Ward, "Comparison of solutions to the scatterometry inverse problem," Proc. SPIE **5375**, 564–576 (2004).
5. G. Cormier and R. Boudreau, "Genetic algorithm for ellipsometric data inversion of absorbing layers," J. Opt. Soc. Am. A **17**, 129–134 (2000).
6. X. Chen, S. Liu, C. Zhang, and J. Zhu, "Improved measurement accuracy in optical scatterometry using fitting error interpolation-based library search," Measurement **46**, 2638–2646 (2013).
7. I. Kallioniemi, J. Saarinen, and E. Oja, "Optical scatterometry of subwavelength diffraction gratings: neural-network approach," Appl. Opt. **37**, 5830–5835 (1998).
8. I. Gereige, S. Robert, and J. Eid, "Automatic detection of photoresist residual layer in lithography using a neural classification approach," Microelectron. Eng. **97**, 29–32 (2012).
9. Z. S. Fawzi, S. Robert, I. E. Kalyoubi, and B. Bayard, "Analysis and detection of an incorrect profile shape in a classical scatterometric process," Eur. Phys. J. Appl. Phys. **76**, 31001 (2016).
10. M. G. Tchéré, S. Robert, Z. S. Fawzi, and B. Bayard, "Reconstruction of a complex profile shape by weighting basic characterization results for nanometrology," Appl. Opt. **58**, 6118–6125 (2019).
11. Z. S. Philippe, S. Robert, and B. Bayard, "Automatic inspection of a residual resist layer by means of self-organizing map," Opt. Eng. **55**, 054106 (2016).
12. J. Zhu, S. Liu, C. Zhang, X. Chen, and Z. Dong, "Identification and reconstruction of diffraction structures in optical scatterometry using support vector machine method," J. Micro/Nanolithography MEMS MOEMS **12**, 013004 (2013).
13. J. Zhu, S. Liu, C. Zhang, X. Chen, and Z. Dong, "Classification and recognition of diffraction structures using support vector machine in optical scatterometry," Proc. SPIE **8324**, 83242S (2012).
14. O. Acher, E. Bigan, and B. Drevillon, "Improvements of phase-modulated ellipsometry," Rev. Sci. Instrum. **60**, 65–77 (1989).
15. M. G. Moharam and T. K. Gaylord, "Rigorous coupled-wave analysis of planar-grating diffraction," J. Opt. Soc. Am. **71**, 811–818 (1981).
16. C.-H. Ko, Y. Ku, and N. Smith, "Correlation of scatterometry sensitivities to variation in device parameters," Proc. SPIE **6152**, 615220 (2006).